

Structure Analysis of OMC1 Filaments at 1.1 mm Emission

Soyoung Youn^A and Sungeun Kim^{A,B}

^A Astronomy and Space Science Department, Sejong University, 143-747, Seoul, Republic of Korea

^B Email: sek@sejong.ac.kr

Abstract: We present a 1.1 mm emission map of the OMC1 region observed with AzTEC, a new large-format array composed of 144 silicon-nitride micromesh bolometers that was in use at the James Clerk Maxwell Telescope (JCMT). The AzTEC observations of the OMC1 region at 1.1 mm reveal dozens of cloud cores and a tail of filaments in a manner that is almost identical to the submillimeter continuum emission of the entire OMC1 region at 450 and 850 μm . The density power spectrum provides the size distribution of the structures. We find that a single power law might be fitted to the calculated power spectrum of the 1.1 mm emission between 0.3 pc and 0.03 pc. The slope of the best fit power law is $\gamma \approx -2.6$ and is similar to the spectral index of the power spectrum of $\gamma \approx -2.7$ found in numerical simulations. However, there is a distinct spectral break in the power spectrum at a characteristic scale of ~ 0.3 pc in OMC1. The effects of beam size and noise spectrum on the shape and slope of the power spectrum are also included in the present analysis. The slope of the power law and a range of different scales change at scales below ~ 0.3 pc as the beam size increases.

Keywords: ISM: submillimeter — ISM: interstellar dust — ISM: power spectrum — ISM: OMC1

1 Introduction

The Orion Nebula is the best-studied massive star-forming region in the nearest giant molecular cloud (GMC) where massive stars have formed, and it has been extensively studied at all wavelengths. The Orion Nebula, M42, is located in the northern part of the Orion A molecular cloud, which consists of OMC1, OMC2, OMC3, and OMC1-S. These components are smoothly connected, and together they form the integral-shaped filaments seen in the optical, infrared, and submillimeter continuum (Johnstone and Bally 1999). OMC1 is the most massive component containing at least 2,000 young stellar objects (YSOs). It exhibits massive star formation, and is strongly connected to the surrounding gas (O'Dell 2001). VLA NH_3 observations revealed the filamentary and clumpy structure of OMC1 (Wiseman and Ho 1996, 1998).

OMC1 has on-going massive star formation and strong interactions between gas and young stellar objects (YSOs), their bipolar stellar jets, and outflows (Mann and Williams 2010; Bally et al. 2011). Submillimeter continuum observations (Lis et al. 1998; Johnstone and Bally 1999) revealed the complex and filamentary structure of the Orion A molecular cloud, especially the Orion Integral-Shaped Filament. Johnstone and Bally (1999) also explored the condensation mass spectrum and derived a temperature distribution for the Orion A cloud. Far-infrared balloon-borne observations of the Orion cloud by Mookerjea et al. (2000) found that the coldest clump in the Orion A cloud had a temperature of about 15 K. Despite various observations of the Orion A cloud over a wide range of wavelengths for over a decade including the SEST SIMBA (Nyman et al. 2001), the 1.1 mm thermal continuum emission arising from OMC1 in the Orion A cloud has recently been observed for the first time, ow-

ing to the development of the Astronomical Thermal Emission Camera (AzTEC), a millimeter-wavelength bolometer array designed for the Large Millimeter Telescope (LMT). AzTEC is composed of an array of 144 nitride micro-mesh composite bolometers (Wilson et al. 2008).

In this paper, we report the results of 1.1 mm AzTEC observations of the OMC1 component of the Orion A cloud. We found that the 1.1 mm emission from OMC1 is distributed in a manner similar to that of the 850 μm emission observed with the Submillimeter Common-User Bolometer Array (SCUBA; Johnstone and Bally 1999). We performed an angular power spectrum analysis (Crovisier and Dickey 1983; Gautier et al. 1992) of the 1.1 mm intensity map, which is dominated by thermal emissions from the relatively cold dust in OMC1. Because dust grains are coupled with gas, elucidating the structure of the dust emission will play an important role in understanding the dynamics and structure of the gas. The large scale properties of turbulence in the interstellar medium (ISM), including those of the gas and dust grains are still poorly understood but the energy input from star formation is thought to be a major driving force for the turbulence in the ISM (Mac Low 2004; Scalo and Elmegreen 2004). The turbulent emission can increase the gas density and initiate star forming instabilities. The generation of the hierarchy of structures (Falgarone, Phillips, & Walker 1991; Elmegreen and Falgarone 1996; Elmegreen, Elmegreen, & Leitner 2003) and flocculent structures (Elmegreen and Elmegreen 1984) present across a range of spatial scales in the ISM (Kim et al. 1998) is also attributed to turbulent emission. Thus, it is important to confirm the slope of the power spectrum of the intensity fluctuations and velocity fields (Stanimirović et al. 1999; Burkert and Bodenheimer 2000; Elmegreen, Kim, &

Staveley-Smith 2001; Stanimirović and Lazarian 2001; Padoan et al. 2006). Any correlation, if present, will provide an insight into the processes that drive turbulence in the ISM (Elmegreen et al. 2001; Heyer and Brunt 2004; Mac Low 2004; Scalo and Elmegreen 2004; Field, Blackman, & Keto 2009; Pineda et al. 2010) and a clue to the presence of fractal or non-fractal structure of the ISM (Blitz and Williams 1997; Hartmann 2002; Brunt 2010). The analysis results are reported in Section 3.

2 Observations and Data

The observations were performed in raster-scan mode between 28 December 2005 and 1 January 2006 using AzTEC mounted on the James Clerk Maxwell Telescope (JCMT), giving a beam size of 18 arcsec and a scan velocity of 120 arcsec s^{-1} . A total integration time of 102.9 seconds was used. From a total of 10 scan maps, five scans were retrieved and combined, covering a total observed area of 655.35 arcmin², which corresponds to about 3.14×3.14 pc². Average RMS was 0.22 mJy. This region was centered on RA=05^h35^m14.4^s, DEC=05°22′32.3″ in J2000. AzTEC suffered a pointing error of 2″. Beam maps were made from observations of Uranus with a mean flux density of 42.2 Jy at 1.1 mm during the JCMT observing run. A pointing model was generated using CRL618, a post-asymptotic giant branch (post-AGB) star with a mean flux density of 2.7 Jy at 1.1 mm. The intensity calibration errors were estimated to be about ± 6 -13% (Wilson et al. 2008). The raw bolometer data were calibrated and edited in IDL (Perera et al. 2008; Scott et al. 2008; Wilson et al. 2008; Austermann et al. 2009).

Each AzTEC data set can be regarded as being in the time sector (i.e., using the data storage method; since all data are stored as a function of time, they are also referred to as time-stream data) and also in the spatial sector. Each observed data set i , M_i is composed of the atmospheric signal, A_i , the astronomical signal, S , and the noise, N_i , in the spatial sector. An astronomical signal estimator, \tilde{S}_i , is built by cleaning the raw data m_i , the time-domain analogs of the M_i . For extended sources, S correlates with the time-stream signals as A_i . The atmosphere, a_i (time-domain analogs of A_i in the time sector) may not be orthogonal to the true sky signal in the time sector, s . An iterative technique was developed to maximize the orthogonality between the principal components being cut from time-stream data and the real astronomical signal. This means that detections of flux in the initial map are subtracted from the raw data. Then, the data streams are cleaned and mapped again. Any significant detections in the second map are added to the source model of the first map, and the summed model is then subtracted from the initial bolometer signals. An iterative cleaning algorithm was performed using the following procedure: 1) set of \tilde{S}_i is found from the set of m_i . \tilde{S} was created by co-adding all the \tilde{S}_i ; 2) \tilde{r}_i , the estimator for the time-stream data unrelated to astronomical signal, is created by subtracting \tilde{s} from m_i ; 3) \tilde{r}_i is cleaned and maps created for the

set of \tilde{R}_i ; these are co-added to find \tilde{R} , the residual map of the sky signal; 4) a new estimator of the true sky signal, \tilde{S}' is created by adding the residual map, \tilde{R} to the map from step 1, \tilde{S} ; 5) we return to step 2 and subtract \tilde{s}' from the input time streams. The final AzTEC images of the OMC1 were the result of 30 iterations. Any induced artifacts from the cleaning processes were compensated for by the inverse effects of any subtracted non-real features in the time stream data. This process was repeated 30 times until the result converged to a model-subtracted map.

3 Results and Discussion

3.1 Fourier Analysis

We present observations of 1.1 mm emission from the OMC1 in the Orion A cloud using a newly developed bolometer camera, AzTEC in Figure 1. The thermal dust emission from cool dust at 1.1 mm is the result of heating from intermediate mass stars (5–20 M_{\odot}) and the interstellar radiation field. The morphology of the 1.1 mm emission arising from the thermal dust radiation in OMC1 is very similar to that of the 850 μ m emission of OMC1 seen with the SCUBA at the JCMT (Johnstone and Bally 1999). Figure 1 presents the morphology of the 1.1 mm dust continuum emission from OMC1. The northern peak is associated with Orion KL (Kleinmann and Low 1967; Allen and Burton 1993; Menten and Reid 1995; Lee and Burton 2000; Zapata et al. 2011), and the southern peak corresponds to the Orion S source (Schmid-Brügk et al. 1990). Their peak fluxes are measured and presented in Table 1.

Table 1: Emission properties for Orion KL and Orion S at 1.1mm

	AzTEC Coordinate		Peak Flux
	RA[J2000]	DEC[J2000]	[Jy/beam]
Orion KL	05:35:14.17	-05:22:33.35	63.9
Orion S	05:36:13.52	-05:24:07.35	26.8

Characterizing the statistical properties of interstellar emission is crucial to understanding the physics and structure of the interstellar medium (ISM). Hence, we performed an angular power spectrum analysis of the intensity map which was dominated by thermal emission from the relatively cold dust in OMC1 (Figure 1). This analysis is frequently used to study the statistical properties of pre-stellar cores in molecular clouds as well as in cosmic microwave background (CMB) and cosmic infrared background (CIB) radiation analysis. The power spectrum has also been used extensively in structure analysis of images. The main goal of this analysis is to place some constraints on the density structure of the interstellar dust emission arising from the OMC1 in the Orion A molecular cloud using Fourier analysis (Bracewell 1986). The mean

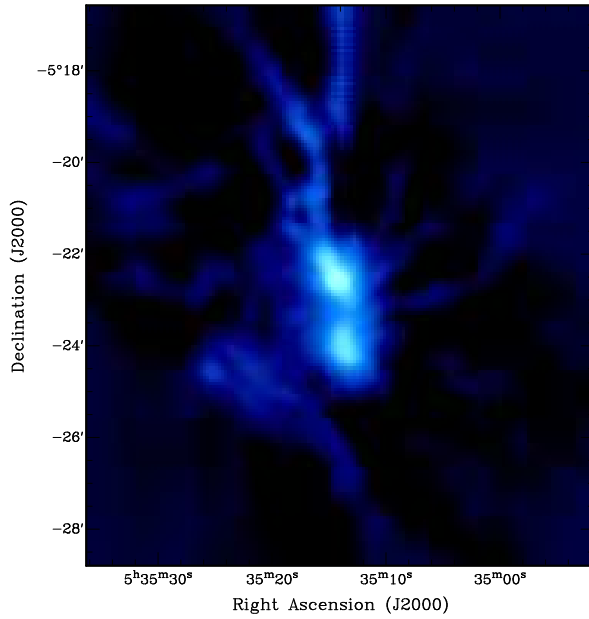


Figure 1: The AzTEC 1.1 mm emission from the OMC1 in the Orion A molecular cloud. The peak flux of the 1.1 mm emission is 63.9 Jy/beam. The calibration error is about 6 – 13% of the flux (Wilson et al. 2008).

power spectrum of the 1.1 mm dust emission from OMC1 is shown in Figure 2. The power spectrum, $P(k)dk$, comes from the Fourier transform of the autocorrelation of the image (Bracewell 1986; Press et al. 1992). Welch’s modified periodogram method (Welch 1967; Press et al. 1992) was applied to the estimate of the power spectrum of the dust continuum image of OMC1 at 1.1 mm. The entire image of OMC1 was used for calculating the power spectrum, $P(k)$, after the edge was trimmed.

$$A(k_x, k_y) = F(k_x, k_y)F^*(k_x, k_y) = |F(k_x, k_y)|^2 \quad (1)$$

This is an angular average of $A(k_x, k_y)$ between k and $k + dk$, where an annulus at $k = \sqrt{k_x^2 + k_y^2}$. It retains some of the spatial characteristics of the projected density field. The two-dimensional Fourier transforms were used to compute the mean power spectrum, $P(k)$, of the entire OMC1 image at 1.1 mm emission by averaging the annulus defined at $k = \sqrt{k_x^2 + k_y^2}$ (Bracewell 1986; Press et al. 1992). This was done by modifying the code (Kim et al. 1999) for analysis of one-dimensional power spectra. Taking the Fourier transform of the autocorrelation resulted in an estimate of the power spectrum, $P(k)$, and the power spectra were summed into rings of constant, k . In the present analysis, the nonparametric periodogram estimator (equation 2) was used for the Fourier transform of the image. The Fourier transform of the product of the data with the window function reflects the convolution of the Fourier transform of the data with the

window function (Bracewell 1986; Press et al. 1992).

$$P(w, N) = \sum_{k=-N+1}^{N-1} r_x(k)e^{-2\pi i k w} \quad (2)$$

The periodogram estimate of the power spectrum, $P(w, N)$, is defined at $N/2 + 1$ frequencies in equation (2). The data were partitioned into K segments and each of $2M$ consecutive points at a number of discrete frequencies. Here, N is $2M$. The periodogram estimates were averaged at each frequency, which reduced the variance of the estimates by a factor of K . Welch’s modified periodogram is justified in equation (3). The expected value of the periodogram converges to the power spectrum in the mean squared sense.

$$P(w) \approx \frac{1}{KL} \sum_{i=0}^{K-1} \left| \sum_{n=0}^{L-1} w(n)x(n+iD)e^{-2\pi i n w} \right|^2 \quad (3)$$

where the overlap occurs at $L - D$ data points and $N = L + D(K - 1)$ (Press et al. 1992). The variance of the periodogram estimate can be defined as

$$\sigma^2 = \frac{1}{L} \sum_{n=0}^{L-1} |w(n) - \mu|^2 \quad (4)$$

where $w(n)$ refers to a window and μ indicates a mean. When the segments are overlapped by one half of their length, the variance of Welch’s periodogram reaches an optimal value, reducing the variance by a factor of about $18K/22$ (Welch 1967; Press et al. 1992). If there is an increase in the number of subsequences to be averaged, then the variance of the estimate is reduced significantly. Therefore, *the power spectrum estimation is approximately unbiased*.

3.2 Power Spectra

We found that it was difficult to fit a single power law to the observed spectrum in Figure 2. The large-scale power law is shallow because it connects to the large-scale portion, while the power spectrum is dominated by the size and shape of the map. The power spectrum obtained from the intensity map of the OMC1 in the present study between 0.3 pc and 0.03 pc follows a power law with a spectral index of γ near -2.6 . This result is similar to the spectral indices of power spectra, $\gamma \approx -2.7$ found in numerical simulations (Padoan et al. 2004) within the error estimate of the power spectrum of the noise (Figure 2). However, there is a distinct spectral break at a characteristic scale of ~ 0.3 pc and possibly at ~ 1.1 pc. The break in the power spectrum occurring at the thickness of the disk was noted in Elmegreen, Kim, & Staveley-Smith (2001). On the other hand, the preferred scale apparent in the power spectrum was also discussed by Brunt (2010) and in the previous studies by Blitz and Williams (1997) and Hartmann (2002).

At smaller scales the observed power spectrum of the image representing the 1.1 mm emission from OMC1 approaches the noise level. Estimates of the power

spectra at smaller scales can often underestimate the value, since structures can be suppressed below the sonic scale (Vázquez-Semadeni, Ballesteros-Paredes, & Klessen 2003). From the present analysis of the OMC1 filaments at 1.1 mm emission (Figure 2), the power spectrum steepens at relatively smaller scales. At the largest scales, the power spectrum flattens. The logarithmic slopes of the power-law spectra obtained for the 1.1 mm emission from OMC1 seem to be lower than the logarithmic slope of a Kolmogorov spectrum. A Kolmogorov spectrum has a power law with logarithmic slope of $11/3$, conventionally taken as evidence for turbulent fluctuations with dynamical energy exchange between irregularities of different scales. These values are also rather lower than the spectral indices of the power spectrum of the dust emission derived in other studies (Gautier et al. 1992). Most spectral indices measured in other studies such as Cirrus cloud studies, range from -3.6 to -2.5 . Often spectra with a logarithmic slope of four or more are caused by deterministic structures. However, it is difficult to explain the power source forming these structures.

Recent studies of turbulence indicate a rather shallow slope of the density power spectrum. For example, Padoan et al. (2004) and Kritsuk and Norman (2004) found slopes somewhat smaller than 1 in their magnetohydrodynamic (MHD) turbulence. In the transonic turbulence model, the density distribution is often generated by discontinuities created by weak shocks overlaid on the turbulence background. In the supersonic turbulence (Burkert 2006), the density distribution is characterized by peaks, or mass concentrations generated by strong shocks (Williams, Blitz, & McKee 2000). As the Mach number increases, the power spectrum slope flattens, and density concentrations appear as sheets and filaments (Wiseman and Ho 1996; Staveley-Smith et al. 1997; Kim et al. 1998; Johnstone and Bally 1999; Kim et al. 1999; Stanimirović et al. 1999). To interpret these results in terms of the density structure, velocity distributions (Williams et al. 1994; Goodman et al. 1998; Ostriker et al. 1999; Elmegreen et al. 2001; Heyer and Brunt 2004; Lazarian, Vishniac, & Cho 2004; Mac Low 2004; Scalo and Elmegreen 2004; Balsara and Kim 2005; Hennebelle and Chabrier 2008; Fukui et al. 2009; Brunt 2010; Burkhart, Lazarian, & Gaensler 2011) and topology of the ISM (Kim and Park 2007) and in comparison with deductions from gas tracers the results should be reproduced by considering a model spectra based on the 1.1 mm emission which is dominated by the gray-body emission from large dust grains at thermal equilibrium temperature. Here, the large grain equilibrium temperature is related to the local radiation field strength and spectrum, which depends on the presence or absence of nearby heat sources as well as extinction. Since grain structure variation and size distribution of interstellar grains can affect the emissivity coefficient and result in variation of the equilibrium dust temperature, this will consequently constrain the pattern of the power spectra at smaller and intermediate scales in the interstellar dust medium.

To understand the observed shape of the power spectrum, we attempted to analyze the impact of vari-

ations in the beam size on the pattern of the observed power spectrum of the OMC1 image at 1.1 mm. We performed power spectrum calculations using three different aperture diameters: $18''$, $36''$, and $55''$. Here, the aperture diameter is an average for the observed region. Despite differences in the details, the power spectra of the 1.1 mm emission at apertures of different sizes are similar in shape. However, the power decreases significantly as the size of the aperture increases (Figure 2). The power spectrum is slightly less steep towards the large beam at relatively small scales, compared to the large-scale structure of OMC1 at 1.1 mm. The slope of the observed power spectrum is more affected by the beam convolution. The power spectra at lower and higher resolutions have a similar appearance at scales above ~ 0.3 pc. But the slope changes significantly at scales below ~ 0.3 pc as the aperture diameter increases. The break in the power spectrum that occurs at the thickness of the disk was noted by Elmegreen, Kim, & Staveley-Smith (2001). However, as we mentioned above, there are also studies of the non-hierarchical structures seen in the molecular clouds (Blitz and Williams 1997; Hartmann 2002; Brunt 2010). The average error in the noise is also measured in terms of the spatial power spectrum, and is presented in Figure 2. The noise includes $1/f$ noise (Wilson et al. 2008) and confusion noise from the background. The shape of the power spectrum for the noise follows a power law and the present analysis yields a spectral index of $\gamma \approx -0.6$ above the scale of 0.1 pc.

4 Summary

We presented a 1.1 mm emission map of the OMC1 region observed with AzTEC, a new large-format array composed of 144 silicon-nitride micromesh bolometers that was in use at the JCMT. We performed Fourier analysis of the image with a modified periodogram, and discussed the density power spectrum including the size distribution of the structures. We noted that there was a distinct spectral break in the power spectrum at a characteristic scale of ~ 0.3 pc and possibly at ~ 1.1 pc in OMC1. However, we were able to fit a single power law to the power spectrum of the 1.1 mm emission map between 0.3 pc and 0.03 pc. The effects of beam size on the shape and slope of the power spectrum were also included in the present analysis. The slope of the power law and a range of different scales appeared to change at the scales below about ~ 0.3 pc as the beam size increased.

Acknowledgments

We appreciate G. Wilson (AzTEC PI), M. Yun, and D. Hughes for observing and help for the data reduction. We are grateful to the AzTEC team members and P. Schloerb for their support. We thank K. Jeong for very helpful suggestions on the manuscript. We would like to thank the anonymous referee for careful reading and critical comments. The James Clerk Maxwell Telescope is operated by the Joint Astronomy Center on behalf of SRC of the United Kingdom, the

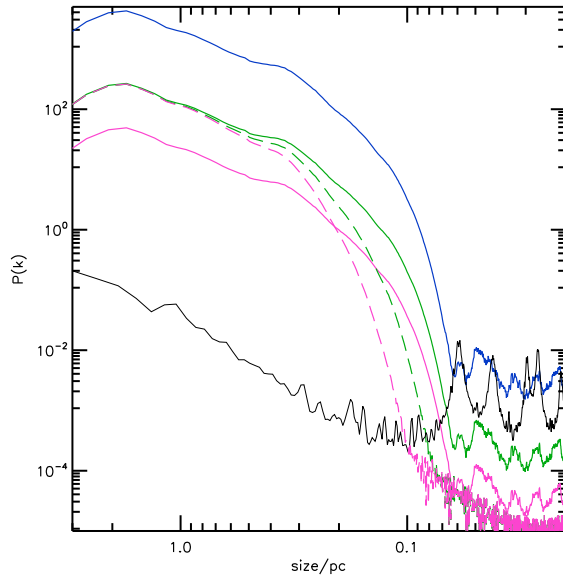


Figure 2: The density power spectrum of the AzTEC 1.1 mm emission from OMC1 was presented. Estimate of the power spectrum was calculated with different aperture diameters of 18'' (blue), 36'' (green solid), 55'' (pink solid), and the noise (black) for the comparison. We also compared the results of analysis for the beam convolution (dashed lines).

Netherlands OSR, and the Canada NRC. The earlier work on the project was supported in part by the Korea Science & Engineering Foundation (KOSEF) under a cooperative agreement with the Astrophysical Research Center of the Structure and Evolution of the Cosmos (ARCSEC). This work was supported in part by the faculty research fund of Sejong University in 2009. This research was also supported in part by Mid-career Researcher Program through the National Research Foundation of Korea (NRF) funded by the Ministry of Education, Science and Technology 2011-0028001.

References

- Allen, D.A., & Burton, M.G. 1993, *Nature*, 363, 54
- Austermann, J.E., Aretxaga, I., Hughes, D.H. et al. 2009, *MNRAS*, 393, 1573
- Balsara, D.S., & Kim, J.S. 2005, *ApJ*, 634, 390
- Blitz, L., & Williams, J.P. 1997, *ApJ*, 488, L145
- Bracewell, R. 1986, *The Fourier Transform and Its Applications* (McGraw-Hill, New York), p. 113
- Brunt, C.M., & Heyer, M.H. 2002, *ApJ*, 566, 289
- Brunt, C.M. 2010, *A&A*, 513, 67
- Burkert, A., & Bodenheimer, P. 2000, *ApJ*, 543, 822
- Burket, A. 2006, *Comptes Rendus-Physique*, 7, 433
- Burkhart, B., Lazarian, A., & Gaensler, B.M. 2011, arXiv1111.3544
- Crovisier, J., & Dickey, J.M. 1983, *A&A*, 122, 282
- Elmegreen, D.M., & Elmegreen, B.G. 1984, *ApJS*, 54, 127
- Elmegreen, B.G., & Falgarone, E. 1996, *ApJ*, 471, 816
- Elmegreen, B.G., Kim, S., & Staveley-Smith, L. 2001, *ApJ*, 548, 749
- Elmegreen, B.G., Elmegreen, D.M., & Leitner, S.N. 2003, *ApJ*, 590, 271
- Falgarone, E., Phillips, T.G., & Walker, C.K. 1991, *ApJ*, 378, 186
- Field, G., Blackman, E., & Keto, E. 2009, arXiv0904.4077F
- Fukui, Y., Kawamura, A., Wong, T., et al. 2009, *ApJ*, 705, 144
- Gautier, T.N., III, Boulanger, F., Perault, M., Puget, J.L. 1992, *AJ*, 103, 1313
- Goodman, A.A., Barranco, J.A., Wilner, D., and Heyer, M.H. 1998, *ApJ*, 504, 223
- Hartmann, L. 2002, *ApJ*, 578, 914
- Hennenelle, P., & Chabrier, G. 2008, *ApJ*, 684, 395
- Heyer, M.H., & Brunt, C.M. 2004, *ApJ*, 615, 45
- Johnstone, D., & Bally, J. 1999, *ApJ*, 510, L49
- Kim, S., Staveley-Smith, L., Dopita, M.A., Sault, R.J., Freeman, K.C., Kesteven, M., McConnell, D. 1998, *ApJ*, 503, 674
- Kim, S., Dopita, M.A., Staveley-Smith, L., & Bessell, M.S. 1999, *AJ*, 118, 2797
- Kim, S. 1999, PhD thesis, The Australian National University, Chapter 2.
- Kim, S., & Park, C. 2007, *ApJ*, 663, 244
- Kleinmann, D.E., & Low, F. 1967, *ApJ*, 149, L1
- Kritsuk, A.G., & Norman, M.L. 2004, *ApJ*, 601, L55
- Lazarian, A., Vishniac, E.T., & Cho, J. 2004, *ApJ*, 603, 180
- Lee, J.-K., & Burton, M.G. 2000, *MNRAS*, 315, 11
- Lis, D.D., Serabyn, E., Keene, J., Dowell, C.D., Benford, D.J., Phillips, T.G., Hunter, T.P., Wang, N. 1998, *ApJ*, 509, 299

- Mac Low, M.M. 2004, *Ap&SS*, 289, 323
- Mann, R.K., & Williams, J.P. 2010, *ApJ*, 725, 430
- Menten, K.M., & Reid, M.J. 1995, *ApJ*, 445, L157
- Mookerjea, B., Ghosh, S.K., Rengarajan, T.N., Tandon, S.N., & Verma, R.P. 2000, *ApJ*, 120, 1954
- Nyman, L.-Å., Lerner, M., Nielbock, M., Anciaux, M., Brooks, K., Chini, R., Albrecht, M., Lemke, R., Kreysa, E., Zylka, R., et al. 2001, *Msngr*, 106, 40
- O'Dell, C.R. 2001, *AJ*, 122, 2662
- Ostriker, E.C., Gammie, C.F., & Stone, J.M. 1999, *ApJ*, 513, 259
- Padoan, P., Kim, S., Goodman, A.A., & Staveley-Smith, L. 2001, *ApJL*, 555, 33
- Padoan, P., Jimenez, R., Nordlund, A., Boldyrev, S. 2004, *PhRvL*, 92, s1102
- Padoan, P., Juvela, M., Kritsuk, A., Norman, M.L. 2006, *ApJ*, 653, 125
- Perera, T.A., Chapin, E.L., Auermann, J.E. et al. 2008, *MNRAS*, 391, 1227
- Pineda, J., Goodman, A., Arce, H.G. et al. 2010, *ApJ*, 712, 116
- Press, W.H., Teukolsky, S.A., Vetterling, W.T., & Flannery, B.P. 1992, *Numerical Recipes in C* (Cambridge University Press), p. 500 - p. 558
- Scalo, J.M., & Elmegreen, B.G. 2004, *ARA&A*, 42, 275
- Schmid-Brugk, J., Güsten, R., Mauersberger, R., Schultz, A., & Wilson, T.L. 1990, *ApJ*, 362, 25
- Scott, K.S., Auermann, J.E., Perera, T.A. et al. 2008, *MNRAS*, 385, 2225
- Stanimirović, S., Staveley-Smith, L., Dickey, J.M., Sault, R.J., & Snowden, S.L. 1999, *MNRAS*, 302, 417
- Stanimirović, S., & Lazarian, A. 2001, *ApJ*, 551, 53
- Staveley-Smith, L., Sault, R.J., Hatzidimitriou, D., Kesteven, M.J., & McConnell, D. 1997, *MNRAS*, 289, 225
- Welch, P.D. 1967, *IEEE Transactions on Audio and Electroacoustics*, 15, 70
- Williams, J.P., de Geus, E.J., & Blitz, L. 1994, *ApJ*, 428, 693
- Williams, J.P., Blitz, L., & McKee, C. 2000, *Protostars and Planets IV* (Tucson: University of Arizona Press; eds Mannings, V., Boss, A.P., Russell, S.S.), p. 97
- Wilson, G.W., Auermann, J.E., Perera, T.A. et al. 2008, *MNRAS*, 386, 807
- Wiseman, J.J. & Ho, P.T.P. 1996, *Nature*, 382, 139
- Wiseman, J.J. & Ho, P.T.P. 1998, *ApJ*, 502, 676
- Zapata, L. A., Schmidt-Burgk, J., & Menten, K.M. 2011, *A&A*, 529, 24